Hydrogen Bond-Assisted Dual Passivation for Blue Perovskite Light-Emitting Diodes

Zhongkai Yu[1], Xinyu Shen[1,2,*], Xiangyang Fan[3], Young-Kwang Jung[4], Woo Hyeon Jeong[1], Akash Dasgupta[2], Manuel Kober-Czerny[2], Pietro Caprioglio[2], Sung Heum Park[3], Hyosung Choi[5], Henry J. Snaith[2], Samuel D. Stranks[4], Bo Ram Lee[1,*]

[1]School of Advanced Materials Science and Engineering, Sungkyunkwan University, Suwon 16419, Republic of Korea

[2]Clarendon Laboratory, Department of Physics, University of Oxford, Oxford OX1 3PU, UK

[3]Department of Physics, CECS Research Institute, and Core Research Institute, Pukyong National University, Busan 48513, Republic of Korea

[4]Department of Chemical Engineering and Biotechnology, University of Cambridge, Cambridge CB3 0AS, UK

[5]Department of Chemistry, Research Institute for Convergence of Basic Sciences, and Research Institute for Natural Science, Hanyang University, Seoul 04763, Republic of Korea

*Corresponding author, E-mail: shenxinyu93@gmail.com, brlee@skku.ac.kr

ABSTRACT

Although significant progress has been made in the development of green, red, and near-infrared perovskite light-emitting diodes (PeLEDs), blue PeLEDs exhibit inferior performance owing to various defects and poor carrier injection in solution-processed perovskite films. Thus, this study incorporates dual-passivation additive diphenylphosphinamide (DPPA) into perovskite films, and through DFT calculations and experimental characterizations, DPPA is proven an effective passivator. Its phosphine oxide group coordinates with unsaturated lead ions, passivating perovskite defects, while the amino group forms hydrogen bonds with adjacent halide ions, suppressing their migration and further strengthening the passivation effect. Blue quasi-2D PeLEDs based on DPPA-modified perovskite films achieved an external quantum efficiency of 12.31% with an emission peak at 486 nm. Moreover, device operational lifetime was extended by 32% with more stable spectra owing to the decreased defect density and suppressed ion migration in the perovskite film.

TOC GRAPHICS

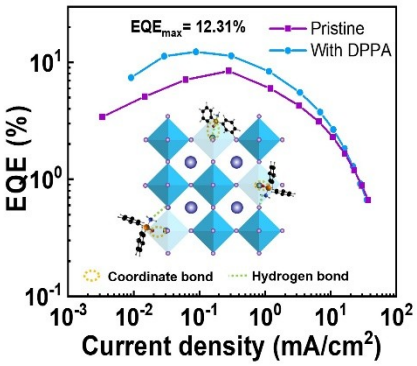

Solution-processable lead halide perovskites are emerging as promising candidates for cost-effective and high-performance light-emitting diodes (LEDs) owing to their outstanding properties such as broadly tuneable emissions, high colour purity, and high photoluminescence quantum yields (PLQYs).[1-9] Although an external quantum efficiency (EQE) of over 20% has been achieved in green-, red-, and near infrared-emitting perovskite LEDs (PeLEDs), the blue PeLEDs exhibit inferior performance, which reduces the development pace of PeLED based display and illumination.[10-17] Quasi-two dimensional (2D) perovskites with strong quantum confinement and quantum well structures stand out as the blue light emitters among the perovskite family, which are benefiting to boost the radiative efficiency and energy transfer within the LEDs.[18-21] However, the EQE of quasi-2D blue PeLEDs is still not as high as that of others due to various defects including deep chloride defects, nonradiative uncoordinated lead ions, and poor carrier injection in solution-processed perovskite films.[22-24]

It has been demonstrated that the device performance can be improved by the device engineering optimization. Modified the interface between the charge transport layer and the perovskite can effectively improve LED performance; for example, the EQE of deep-blue PeLEDs with an emission at 469 nm was raised to 4.14% by utilizing the K^+ inorganic salt-modified hole transport layer (HTL) to boost carrier injection and the control crystal orientation.[25] Meanwhile, optimizing perovskite emission greatly contributes to enhance LED performance. For instance, a sky-blue LED emitting at 488 nm, obtained by substituting Cs^+ cations with ethylammonium (EA) cations to form the $PEA_2(Cs_{1-x}EA_xPbBr_3)_2PbBr_4$, demonstrated a PLQY of over 70% and 12.1% EQE.[26] The introduction of additives with ionic, coordinate, and hydrogen bonds and core-shell structure to passivate perovskite defects has been shown to improve the LED efficiency, among which Lewis base additives have been reported to have outstanding passivating effects.[27-30] It is noteworthy that single passivation is not sufficiently thorough, and zwitterion additives with multiple functional groups exhibit superior optimization effects due to synergetic effect. Liu *et al.* recently fabricated high-performance sky-blue PeLEDs emitting at 490 nm with a recorded EQE of 15.6% by introducing zwitterions with two functional groups into the perovskite precursors to coordinate the unsaturated Pb^{2+} and control

the perovskite crystallization kinetics.[31] However, the synergetic dual passivation using molecules with multiple functional groups is still insufficiently explored.

Here, we rationally introduce diphenylphosphinamide (DPPA) as a dual-passivation additive into quasi-2D perovskite films to form coordination and hydrogen bonds with perovskite simultaneously. This achieves a significant improvement in the optoelectronic performance of perovskite films through the passivation of nonradiative recombination defects. The auxiliary effect of hydrogen bonding further strengthens the passivation and suppresses ion migration. In addition, the binding of DPPA with perovskite optimizes the phase distribution of the quasi-2D perovskite, which is conducive to radiative recombination. Consequently, the PLQY of the quasi-2D $CsPbBr_3$+PEACl perovskite film was improved from 40.2% for the pristine film to 54.5% for the DPPA passivated film. Correspondingly, the peak EQE of the blue quasi-2D PeLEDs was improved to 12.31% with emission peak at 486 nm.

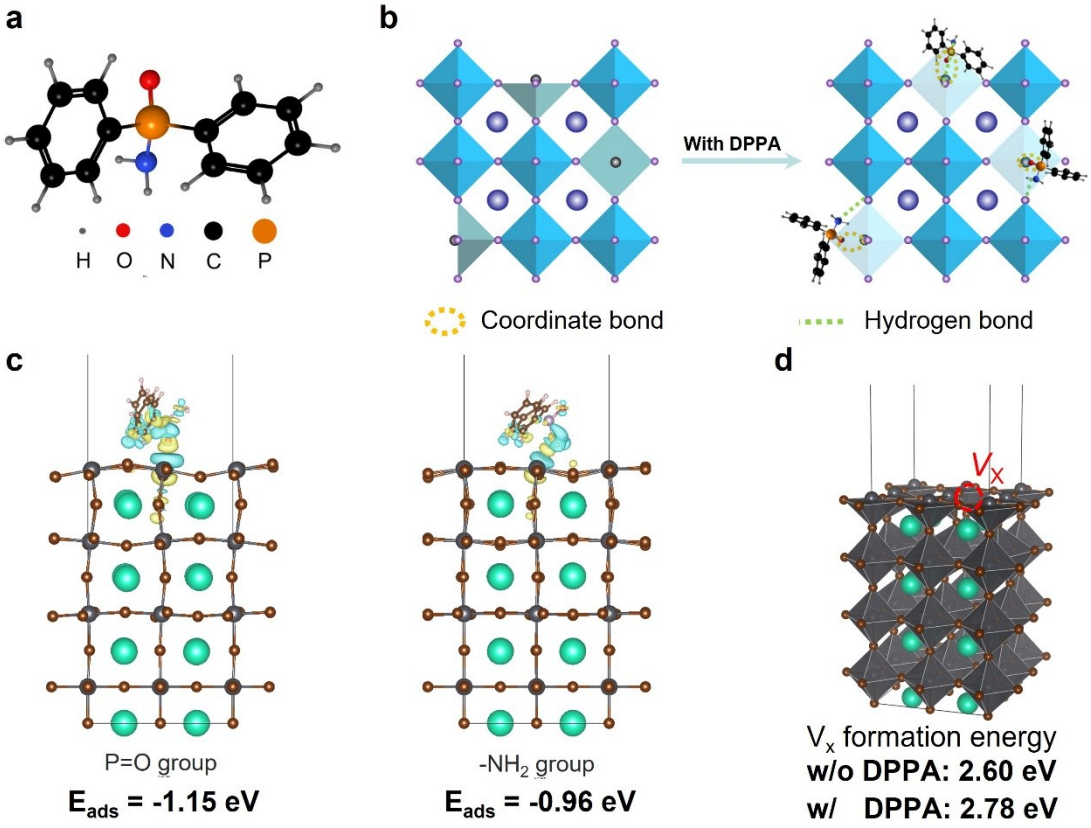

Figure 1. a) Chemical structure of DPPA. b) Schematic illustration of the interaction of DPPA with perovskite. c) Adsorption energy of P=O group and -NH_2 group with perovskite. Yellow and blue clouds show electron accumulation and depletion regions, respectively. d) Formation energy of halide vacancy on the surface without and with DPPA.

Considering the various passivation mechanisms, the organic molecule DPPA, whose chemical structure containing amino group and phosphine oxide group is shown in Figure 1a, was selected as the passivation agent incorporated into the perovskite precursor. DPPA can bind to perovskites through amino group and phosphine oxide groups forming coordinate and hydrogen bonds, as depicted in the schematic illustration of the interaction in Figure 1b. Further density functional theory (DFT) calculations reveal that the adsorption energies of amino and phosphine oxide group onto perovskite are -0.96 eV and -1.15 eV, respectively, which means the P=O group preferentially binds to perovskite more than the NH_2 group does. Additionally, the formation energy of halide vacancy (V_X) in perovskite increases from 2.60 eV to 2.78 eV upon introducing DPPA, implying a suppression effect of DPPA on halide vacancy formation on the surface of halide perovskites. Computational details can be found in the experimental section. As the theoretical analysis presented above, we speculate that the coordination of DPPA and the quasi-2D perovskites occurs predominantly between the P=O group and the unsaturated Pb^{2+} ions, where Lewis base-acid interactions effectively mitigate perovskite defects.[32-35] Meanwhile, the active hydrogen atoms of the -NH_2 group form hydrogen bonds with adjacent halide ions, which further strengthen the passivation effect of DPPA on the perovskite.

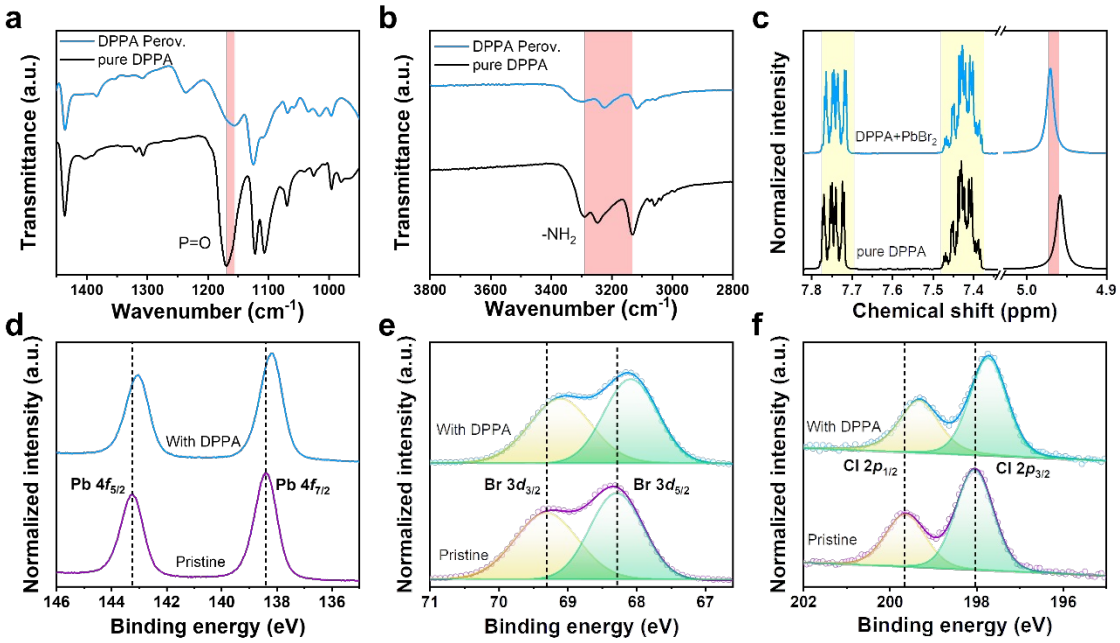

Figure 2. a, b) FTIR spectra of pure DPPA powder and DPPA-incorporated perovskite films. c) ^{1}H-NMR spectra of DPPA and DPPA+$PbBr_2$ in deuterated dimethyl sulfoxide (DMSO-d_6). XPS spectra of pristine and DPPA-incorporated perovskite films of d) Pb 4*f*, e) Br 3*d* and f) Cl 2*p*.

To investigate the DPPA passivation mechanism, we conducted a series of experiments for validation. Fourier-transform infrared spectroscopy (FTIR) was utilized to investigate the interaction mode between perovskite and DPPA. As illustrated in Figure 2a, the stretching vibration peak of the pure DPPA sample is situated at 1170 cm^{-1}, whereas the stretching vibration peak of the sample of perovskite with DPPA is located at 1156 cm^{-1}. The downward shift of the latter confirms the coordination between the P=O group and the perovskite.[36-38] The stretching vibration peaks of amino groups in perovskite with DPPA sample and pure DPPA sample were compared in order to demonstrate the existence of hydrogen bonds. Since the N-H stretching signal can be observed from both PEA^+ and DPPA. To investigate the interaction between DPPA and perovskite without noise signal from the PEA^+, we made the sample with the $CsPbBr_3$ and DPPA for FTIR measurement. As depicted in Figure 2b, the three signal peaks of pure DPPA sample in the highlighted region arise from the asymmetric N-H stretching vibration (3290 cm^{-1}), symmetric N-H stretching vibration (3247 cm^{-1}), and the overtone of the N-H bending vibration (3132 cm^{-1}).[39] In contrast, significant shifts are observed in the amino group peaks of the perovskite with DPPA sample, indicating that the amino group formed hydrogen bonds with the halide ions.

Additionally, ^{1}H nuclear magnetic resonance (NMR) spectroscopy was performed to confirm the hydrogen bonding interaction between DPPA and halide ions. As shown in Figure 2c, the two clusters of split peaks around 7.75 ppm and 7.43 ppm belong to the hydrogen on the phenyl of the DPPA molecule and the signal of the active hydrogen on the amino group is observed at 4.96 ppm, based on the resonance peak areas in the pure DPPA sample. Upon addition of $PbBr_2$, the resonant signal of the active hydrogen on the amino group shifted downfield to 4.97 ppm, indicating the formation of hydrogen bonds between the amino group and halide ions. Furthermore, X-ray photoelectron spectroscopy (XPS) was employed to investigate the binding interaction between DPPA and lead halide octahedra. The core-level peaks of Pb 4*f*, Br 3*d* and Cl 2*p* are displayed in Figure 2d–f; the Pb 4*f* signal peaks of the pristine perovskite sample located at 143.2 eV and 138.4 eV shift toward lower binding energies (143.0 eV and 138.2 eV) upon the introduction of DPPA (Figure 2d). The reduction in the binding energy of Pb 4*f* can be attributed to the empty 6*p* orbital of Pb^{2+} accepting lone pair electrons from the oxygen atom of the P=O group, which serves as strong evidence for the coordination between DPPA and unsaturated Pb^{2+}. Simultaneously, due to the variation in the electrostatic interaction between Pb^{2+} and halide ions (Br^{-}, Cl^{-}), as well as the assisting role of hydrogen bonding, the binding energies of Br 3*d* and Cl 2*p* in the DPPA-incorporated perovskite film is also decreased in comparison to those in the pristine perovskite sample (Figure 2e, f).[40, 41]

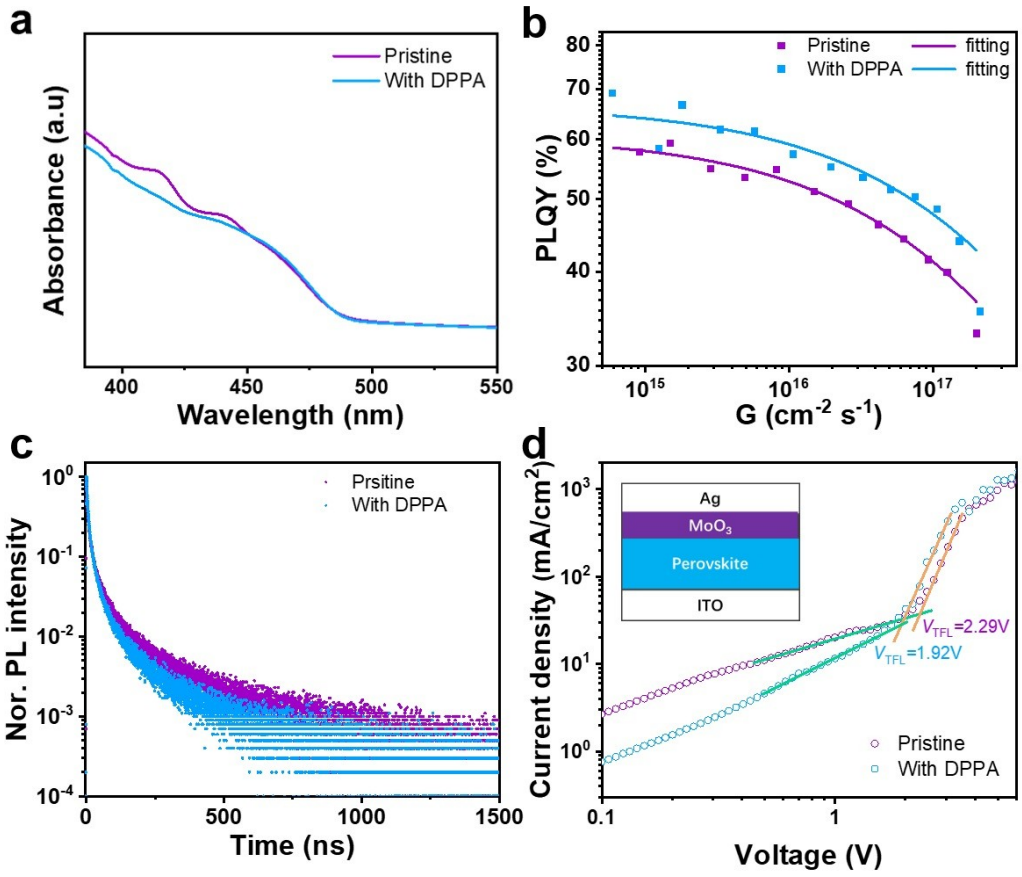

Figure 3. a) UV−vis absorption spectra of pristine and DPPA-incorporated perovskite films. b) The excitation-intensity dependent PLQY. and c) PL decay curves of pristine and DPPA-incorporated perovskite films at the fluence of 241 nJ cm^{-2}. d) Current density-voltage (J–V) curves of hole-only devices without and with DPPA-incorporated.

Subsequently, were explored the optical properties of the pristine perovskite film and DPPA-incorporated perovskite film. As the Ultraviolet−visible (UV−vis) absorption spectroscopy presented in Figure 3a, there are two absorption peaks located at 414 nm and 440 nm, which can be assigned to the n = 2 and n = 3 phases of quasi-2D perovskite, respectively. In quasi-2D perovskites, organic spacers sandwich different numbers of lead halide octahedral layers to form phases with different n values, and stacking of the same phase results in enhanced absorption peak intensity. As observed, the pristine perovskite film exhibits distinct n = 2 and n = 3 phases, which may impede the charge and energy transfer in quasi-2D perovskite film due to the insulating organic spacers.[42] Since the combination with lead halide octahedra disturbs the aggregation of organic spacers, the incorporation of DPPA clearly suppresses the formation of

the n = 2 and n = 3 phases, optimizing the phase distribution of the quasi-2D perovskite film.[7, 31] The decrease in the content of small-n phases implies a shorter pathway for the energy transfer to the recombination center, which is conducive to exciton radiative recombination. In addition, we computed the Urbach energy (E_u) of the two perovskite films from the ln-transformed absorption coefficient versus photon energy plots (Figure S1), employing the following formula: $\alpha(E)=\alpha_0 \exp\left(\frac{E-E_C}{E_u}\right)$,[43] where E represents the photon energy, α represents the absorption coefficient, and α_0 and E_C are material constants. The Urbach energies of the pristine and DPPA-incorporated perovskite samples can be obtained from the inverse slope by fitting the linear part of the curves, are 60.2 meV and 47.7 meV, respectively. The reduced Urbach energy indicates a reduced defect state density.[7, 44-47] Figure S2 shows the PL spectra of the pristine and DPPA-treated perovskite films. The PL intensity of the perovskite film is enhanced significantly with DPPA treatment. Meanwhile, the PLQY with different amount of DPPA are presented in Figure S3, the perovskite with DPPA 10% exhibit the highest PLQY.

To investigate the PL enhancement of the DPPA passivation, we measured the excitation-intensity dependent PLQY of pristine and DPPA passivated perovskite film. As shown in Figure 3b, the DPPA passivated perovskite exhibit higher PLQY than pristine perovskite at different excitation fluence. According to the model: $\frac{dn}{dt}=G-k_{2,r}n^2-k_{2,nrad}n^2-k_3n^3$, where G is the generation rate, $k_{2,r}$ is the rate of radiative bimolecular recombination, $k_{2,nrad}$ is nonradiative second order recombination, and k_3 is the rate of Auger recombination.[48] The fitting rates are listed in Table S1, and the $k_{2,r}$ of perovskite was improved with the DPPA passivation. Meanwhile, the time-resolved photoluminescence (TRPL) decay curves of pristine and DPPA-incorporated perovskite films at different excitation fluence are displayed in Figure 3c and Figure S4. The PL lifetime (τ, the time at which the emission intensity decreases to 1/e of the intensity at t=0) of pristine perovskite is 5.2 ns and 5.5 ns at the fluence is ~ 24 nJ cm^{-2} and 241 nJ cm^{-2}, respectively, while the τ of DPPA passivated perovskite is 6.3 ns and 6.7 ns at the fluence is ~ 24 nJ cm^{-2} and 241 nJ cm^{-2}, respectively. The improvement can be attributed to the effective passivation of the perovskite defects by DPPA. In addition, we fitted the fluence-dependent TRPL in Figure S5, while the fitting data are shown in Table S2 (The details of the fitting are

provided in the Supporting Information). The value of bimolecular recombination calculated from TRPL are of the same order of magnitudes as the $k_{2,r}$ from the excitation-intensity dependent PLQY, suggesting that the radiative bimolecular recombination dominates the PL process. In addition, radiative bimolecular recombination of DPPA passivated perovskite from both methods has been improved compared to the pristine perovskite, indicating that an enhancement of radiative recombination gives contribution to the enhanced PLQY.

The space-charge-limited current (SCLC) curve of hole-only device with a structure of ITO/perovskite/MoO_3/Ag was utilized to characterize the defect density of pristine film and DPPA-incorporated perovskite film. As illustrated in Figure 3d, the trap-filled limit voltage (V_{TFL}) of the DPPA-incorporated perovskite film decreased from 2.29 V in the pristine sample to 1.92 V. The trap state density of perovskite was estimated by the equation of $N_t = (2 V_{TFL} \varepsilon_r \varepsilon_0) / (e L^2)$,[20] where ε_r represents the relative dielectric constant of perovskite, ε_0 is the vacuum permittivity (8.854×10^{-12} F m^{-1}), e represents the elementary electronic charge and L is the thickness of the perovskite layer. The relative trap state density of the pristine perovskite sample was 9.81×10^{17} cm^{-3}, higher than the 8.23×10^{17} cm^{-3} of the DPPA-incorporated sample, indicating that DPPA can effectively passivate perovskite defects. Furthermore, we estimated the hole mobility (μ) of the perovskite layer by employing the Mott-Gurney equation: $J = (9 \varepsilon_r \varepsilon_0 \mu V^2) / (8 L^3)$. The estimated hole mobility is not the absolute hole mobility, but it can be used to investigate electrical properties of perovskite qualitatively. The estimated hole mobility of the pristine perovskite film and DPPA-incorporated perovskite film were 4.81×10^{-6} cm^2 V^{-1} s^{-1} and 5.89×10^{-6} cm^2 V^{-1} s^{-1}, respectively, indicating an improved hole mobility with the passivation of DPPA.

To explore whether the incorporation of DPPA would have an impact on the morphology of the perovskite film, scanning electron microscopy (SEM) was performed. As shown in Figure S6, both the pristine perovskite film and the DPPA-incorporated perovskite film exhibited similar morphologies, with a dense and pinhole-free surface. Additionally, the contact angle images of water on the perovskite film are presented in Figure S7. The contact angle on the pristine film is 45.1°, which increases to 53.9° upon the addition of DPPA. This increase in contact angle confirms the enhanced water repellency of the DPPA-incorporated perovskite film

due to the hydrophobic nature of DPPA. The water-resistant perovskite film is beneficial to the operational stability of the device, which was confirmed as shown further below. Furthermore, X-ray diffraction (XRD) measurements (Figure S8) were performed to study the effect of DPPA on the crystallization of perovskite. Two distinct diffraction peaks at 15.5° and 31.0° can be observed in both pristine and DPPA samples, which can be assigned to the (100) and (200) planes of the bulk phase perovskite. The XRD diffraction peak remained unchanged following the introduction of DPPA, suggesting that DPPA did not penetrate into the perovskite lattice, and the appropriate amount of addition did not affect the crystallinity of perovskite.

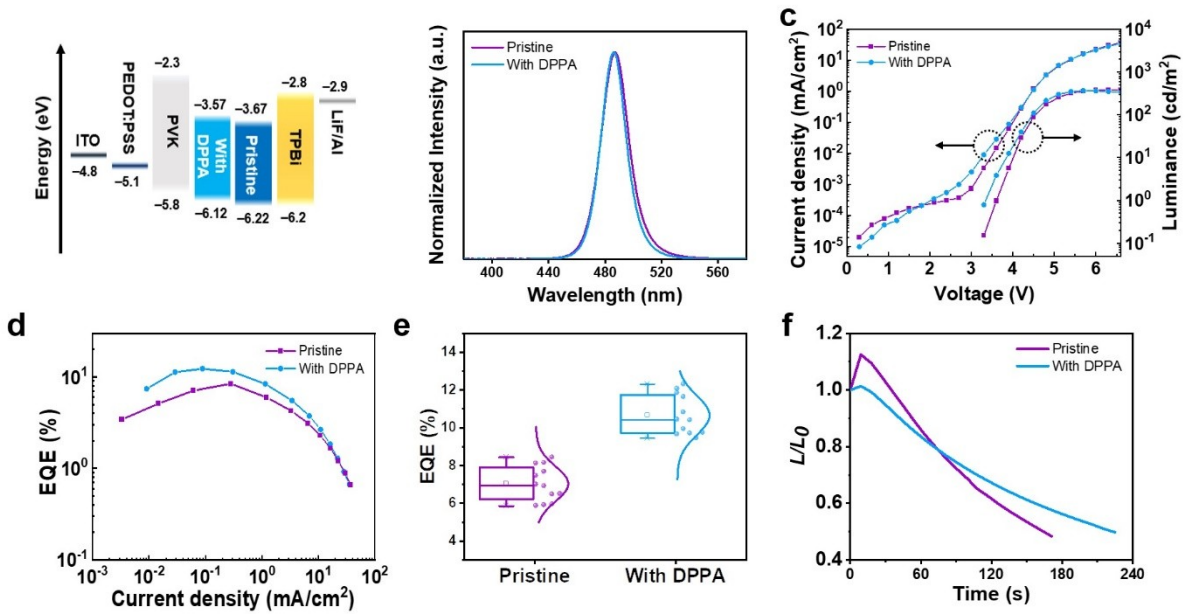

Figure 4. a) Energy level diagram of PeLED. b) Normalized EL spectra for the pristine and DPPA-modified devices. c) Current density-voltage (J-V) curves and luminance-voltage (L-V) curves. d) EQE-current density (EQE-J) curves. e) The statistical maximum EQE values of 12 devices. f) Operational stability for the pristine and DPPA-modified devices.

To explore the application of the two perovskite films in luminescent devices, PeLEDs were fabricated using pristine and DPPA-incorporated perovskite layers (Figure 4). The energy level diagram is illustrated in Figure 4a, with the device architecture consisting of ITO/PEDOT:PSS/PVK/ Perovskite/TPBi/LiF/Al. Compared with that of the pristine perovskite layer, the energy barrier between the HOMO levels of DPPA-modified perovskite layer and HTL

poly(9-vinlycarbazole) (PVK) is smaller, which is beneficial to the hole injection. As determined by ultraviolet photoelectron spectroscopy (UPS) measurement in Figure S9, the secondary electron cutoff energy of perovskite sample increased from 16.94 eV to 17.02 eV after DPPA was introduced. The Fermi levels of the pristine and the DPPA-incorporated perovskite samples were calculated to be -4.28 eV and -4.20 eV, respectively. The DPPA molecules that exist on the perovskite surface bind to Pb^{2+} by donating lone pair electrons, acting as a negative dipole, which decreases the work function of perovskite film.[49] The Fermi edges of the pristine perovskite sample and the DPPA-incorporated perovskite sample are 1.94 eV and 1.92 eV, and the calculated HOMO levels are -6.22 eV and -6.12 eV, respectively. The increased HOMO level reduces the energy barrier between the HTL and EML, which is conducive to the injection of holes. Based on the absorption spectra, we determined an optical bandgap of 2.55 eV for both pristine perovskite and DPPA-incorporated perovskite through the Tauc plot method (Figure S10). This corresponded to electroluminescence (EL) spectra with nearly identical wavelengths (Figure 4b). The normalized EL spectra for the DPPA-modified device and the pristine device with narrow full width at half-maximum, while a wavelength shift of only 1 nm is considered negligible.

Figure 4c, d and Figure S11-12 depict the device characteristics, including current density-voltage (J-V) curves, luminance-voltage (L-V) curves, EQE-current density (EQE-J) curves and EQE-Luminance (EQE-L) curves. As observed in Figure 4c, the DPPA-modified device exhibits lower leakage current in the low voltage region due to reduced defect density, and improved charge injection near the turn-on voltage due to a smaller energy barrier between the HTL and the EML. Therefore, the DPPA-modified device exhibits a maximum external quantum efficiency (EQE) of 12.31% with emission peak at 486 nm, while the highest EQE of the pristine device is only 8.43% with emission peak at 487 nm (Figure 4d). More detailed parameters regarding the device performance are listed in Table S3. Figure 4e shows the statistical maximum EQE values of 12 devices for DPPA-modified and pristine devices, where the average EQE values are 10.54% and 6.94%, respectively. The operational stability of the devices was measured without encapsulation in a glovebox at an initial luminance (L_0) of 30 cd m^{-2}. As shown in Figure 4f, the DPPA-modified device exhibited a longer operational half lifetime compared with the pristine device. Meanwhile, the pristine device showed a significant increase in luminance at the initial stage of operation. This luminance overshoot phenomenon is believed

to be caused by ion migration,[50] which is suppressed in the DPPA-modified device. Based on previous reports,[51] we conducted forward and reverse J-V scans on pristine and DPPA-modified devices. As illustrated in Figure S13, the DPPA-modified device shows a smaller hysteresis loop area, verifying that DPPA can effectively suppress the ion migration and prolong the device lifetime by a hydrogen bond-assisted passivation effect. It is well known that PeLEDs based on mixed halide systems undergo phase segregation under an electric field, leading to unstable emission spectra. The EL spectra of the pristine and DPPA-modified devices at different biases are presented in Figure S14. Both devices display stable EL spectra when the bias voltage is below 6V. However, there is a noticeable redshift in the EL spectra when the bias voltage exceeds 6V. Specifically, the pristine device experiences an 8nm spectral shift, while the DPPA-modified device presents a 4nm shift under overvoltage conditions (Figure S14a and b). When we switch to the current density view, the EL of pristine device redshift from 487 nm to 495 nm with the increasing current density, while the DPPA passivated LED exhibit a 4nm redshift as the current density increasing (Figure S14c and d). That is to say, the ion migration has been suppressed with the DPPA passivation.

In conclusion, we introduced a small molecule additive, DPPA, containing two functional groups to enhance the optoelectronic properties of quasi-2D blue perovskite. Through dual passivation of coordinate bond and hydrogen bond between DPPA and perovskite, the phase distribution has been optimized, boosting the radiative recombination rates and the PLQY of the quasi-2D perovskite. Meanwhile, the injection barrier has been suppressed, as well as the hole mobility was increased. Based on the synergetic effect of dual passivation, quasi-2D blue PeLEDs with superior operational and spectral stability have been achieved with a maximum EQE of 12.31% at 486 nm. Our work provides meaningful guidance for the development of efficient and stable quasi-2D PeLEDs based on mixed halide systems.

ASSOCIATED CONTENT

Supporting Information. Experimental methods, ln(α) vs photon energy plots, PLQY spectra, SEM images, contact angle images, XRD patterns, UPS spectra, Tauc plots, EQE-L curves, J-V curves, EL spectra, device performances.

AUTHOR INFORMATION

Corresponding Authors

Xinyu Shen - School of Advanced Materials Science and Engineering, Sungkyunkwan University, Suwon 16419, Republic of Korea, Republic of Korea; Clarendon Laboratory, Department of Physics, University of Oxford, Oxford OX1 3PU, UK; E-mail: shenxinyu93@gmail.com

Bo Ram Lee - School of Advanced Materials Science and Engineering, Sungkyunkwan University, Suwon 16419, Republic of Korea, Republic of Korea; E-mail: brlee@pknu.ac.kr

Authors

Zhongkai Yu - School of Advanced Materials Science and Engineering, Sungkyunkwan University, Suwon 16419, Republic of Korea, Republic of Korea, Republic of Korea

Xiangyang Fan - Department of Physics, CECS Research Institute, and Core Research Institute, Pukyong National University, Busan 48513, Republic of Korea

Young-Kwang Jung - Department of Chemical Engineering and Biotechnology, University of Cambridge, Cambridge CB3 0AS, UK

Woo Hyeon Jeong - School of Advanced Materials Science and Engineering, Sungkyunkwan University, Suwon 16419, Republic of Korea, Republic of Korea, Republic of Korea

Akash Dasgupta - Clarendon Laboratory, Department of Physics, University of Oxford, Oxford OX1 3PU, UK

Manuel Kober-Czerny - Clarendon Laboratory, Department of Physics, University of Oxford, Oxford OX1 3PU, UK

Pietro Caprioglio - Clarendon Laboratory, Department of Physics, University of Oxford, Oxford OX1 3PU, UK

Sung Heum Park - Department of Physics, CECS Research Institute, and Core Research Institute, Pukyong National University, Busan 48513, Republic of Korea

Hyosung Choi - Department of Chemistry, Research Institute for Convergence of Basic Sciences, and Research Institute for Natural Science, Hanyang University, Seoul 04763, Republic of Korea

Samuel D. Stranks - Department of Chemical Engineering and Biotechnology, University of Cambridge, Cambridge CB3 0AS, UK

Henry J. Snaith - Clarendon Laboratory, Department of Physics, University of Oxford, Oxford OX1 3PU, UK

Author Contributions

Z.Y., X.S. and B.R.L. initiated the project. Z.Y., X.S., W.H.J., and H.C. performed the characterization of the materials and perovskite films. Z.Y. and X.F. fabricated the LED devices and carried out the device performance measurements. Y.K.J. and S.D.S. conducted the DFT calculations. X.S., A.D., M.K.C and P.C carried out the photophysical characterization under the supervision of H.J.S. Z.Y., X.S. and B.R.L. drafted the first version of the manuscript. S.H.P., X.S. and B.R.L. reviewed and revised the manuscript. All the authors participated in the preparation and revision of the manuscript.

Notes

The authors declare no competing financial interest.

ACKNOWLEDGMENT

This work was supported by the National Research Foundation of Korea (NRF-2022H1D3A3A01077343, 2022R1A2C4002248 and 2021M3H4A1A02049006). This research was supported by the core research institute (CRI) program, the basic science research program through the national research foundation of Korea (NRF) under program number (2022R1A6A1A03051158). Thank to Dr. Jeongjae Lee in Seoul National University for the advice on chemical analysis.

REFERENCES

(1) Cho, H.; Jeong, S.-H.; Park, M.-H.; Kim, Y.-H.; Wolf, C.; Lee, C.-L.; Heo, J. H.; Sadhanala, A.; Myoung, N.; Yoo, S.; et al. Overcoming the electroluminescence efficiency limitations of perovskite light-emitting diodes. *Science* **2015**, *350* (6265), 1222-1225.

(2) Ban, M.; Zou, Y.; Rivett, J. P. H.; Yang, Y.; Thomas, T. H.; Tan, Y.; Song, T.; Gao, X.; Credgington, D.; Deschler, F.; et al. Solution-processed perovskite light emitting diodes with efficiency exceeding 15% through additive-controlled nanostructure tailoring. *Nat. Commun.* **2018**, *9* (1), 3892.

(3) Lin, K.; Xing, J.; Quan, L. N.; de Arquer, F. P. G.; Gong, X.; Lu, J.; Xie, L.; Zhao, W.; Zhang, D.; Yan, C.; et al. Perovskite light-emitting diodes with external quantum efficiency exceeding 20 per cent. *Nature* **2018**, *562* (7726), 245-248.

(4) Cao, Y.; Wang, N.; Tian, H.; Guo, J.; Wei, Y.; Chen, H.; Miao, Y.; Zou, W.; Pan, K.; He, Y.; et al. Perovskite light-emitting diodes based on spontaneously formed submicrometre-scale structures. *Nature*

2018, *562* (7726), 249-253.

(5) Zhao, B.; Lian, Y.; Cui, L.; Divitini, G.; Kusch, G.; Ruggeri, E.; Auras, F.; Li, W.; Yang, D.; Zhu, B.; et al. Efficient light-emitting diodes from mixed-dimensional perovskites on a fluoride interface. *Nat. Electron.* **2020**, *3* (11), 704-710.

(6) Yang, L.; Zhang, Y.; Ma, J.; Chen, P.; Yu, Y.; Shao, M. Pure Red Light-Emitting Diodes Based on Quantum Confined Quasi-Two-Dimensional Perovskites with Cospacer Cations. *ACS Energy Lett.* **2021**, *6* (7), 2386-2394.

(7) Liu, Z.; Qiu, W.; Peng, X.; Sun, G.; Liu, X.; Liu, D.; Li, Z.; He, F.; Shen, C.; Gu, Q.; et al. Perovskite Light-Emitting Diodes with EQE Exceeding 28% through a Synergetic Dual-Additive Strategy for Defect Passivation and Nanostructure Regulation. *Adv. Mater.* **2021**, *33* (43), 2103268.

(8) Chiba, T.; Hayashi, Y.; Ebe, H.; Hoshi, K.; Sato, J.; Sato, S.; Pu, Y.-J.; Ohisa, S.; Kido, J. Anion-exchange red perovskite quantum dots with ammonium iodine salts for highly efficient light-emitting devices. *Nat. Photonics* **2018**, *12* (11), 681-687.

(9) Wang, Q.; Wang, X.; Yang, Z.; Zhou, N.; Deng, Y.; Zhao, J.; Xiao, X.; Rudd, P.; Moran, A.; Yan, Y.; et al. Efficient sky-blue perovskite light-emitting diodes via photoluminescence enhancement. *Nat. Commun.* **2019**, *10* (1), 5633.

(10) Kim, Y.-H.; Kim, S.; Kakekhani, A.; Park, J.; Park, J.; Lee, Y.-H.; Xu, H.; Nagane, S.; Wexler, R. B.; Kim, D.-H.; et al. Comprehensive defect suppression in perovskite nanocrystals for high-efficiency light-emitting diodes. *Nat. Photonics* **2021**, *15* (2), 148-155.

(11) Kim, J. S.; Heo, J.-M.; Park, G.-S.; Woo, S.-J.; Cho, C.; Yun, H. J.; Kim, D.-H.; Park, J.; Lee, S.-C.; Park, S.-H.; et al. Ultra-bright, efficient and stable perovskite light-emitting diodes. *Nature* **2022**, *611* (7937), 688-694.

(12) Wang, K.; Lin, Z.-Y.; Zhang, Z.; Jin, L.; Ma, K.; Coffey, A. H.; Atapattu, H. R.; Gao, Y.; Park, J. Y.; Wei, Z.; et al. Suppressing phase disproportionation in quasi-2D perovskite light-emitting diodes. *Nat. Commun.* **2023**, *14* (1), 397.

(13) Hassan, Y.; Park, J. H.; Crawford, M. L.; Sadhanala, A.; Lee, J.; Sadighian, J. C.; Mosconi, E.; Shivanna, R.; Radicchi, E.; Jeong, M.; et al. Ligand-engineered bandgap stability in mixed-halide perovskite LEDs. *Nature* **2021**, *591* (7848), 72-77.

(14) Sun, Y.; Ge, L.; Dai, L.; Cho, C.; Ferrer Orri, J.; Ji, K.; Zelewski, S. J.; Liu, Y.; Mirabelli, A. J.; Zhang, Y.; et al. Bright and stable perovskite light-emitting diodes in the near-infrared range. *Nature* **2023**, *615* (7954), 830-835.

(15) Jiang, J.; Chu, Z.; Yin, Z.; Li, J.; Yang, Y.; Chen, J.; Wu, J.; You, J.; Zhang, X. Red Perovskite Light-Emitting Diodes with Efficiency Exceeding 25% Realized by Co-Spacer Cations. *Adv. Mater.* **2022**, *34* (36), 2204460.

(16) Guo, B.; Lai, R.; Jiang, S.; Zhou, L.; Ren, Z.; Lian, Y.; Li, P.; Cao, X.; Xing, S.; Wang, Y.; et al. Ultrastable near-infrared perovskite light-emitting diodes. *Nat. Photonics* **2022**, *16* (9), 637-643.
(17) Jiang, Y.; Sun, C.; Xu, J.; Li, S.; Cui, M.; Fu, X.; Liu, Y.; Liu, Y.; Wan, H.; Wei, K.; et al. Synthesis-on-substrate of quantum dot solids. *Nature* **2022**, *612* (7941), 679-684.
(18) Wang, Y.-K.; Ma, D.; Yuan, F.; Singh, K.; Pina, J. M.; Johnston, A.; Dong, Y.; Zhou, C.; Chen, B.; Sun, B.; et al. Chelating-agent-assisted control of CsPbBr3 quantum well growth enables stable blue perovskite emitters. *Nat. Commun.* **2020**, *11* (1), 3674.
(19) Li, Z.; Chen, Z.; Yang, Y.; Xue, Q.; Yip, H.-L.; Cao, Y. Modulation of recombination zone position for quasi-two-dimensional blue perovskite light-emitting diodes with efficiency exceeding 5%. *Nat. Commun.* **2019**, *10* (1), 1027.
(20) Ren, Z.; Yu, J.; Qin, Z.; Wang, J.; Sun, J.; Chan, C. C. S.; Ding, S.; Wang, K.; Chen, R.; Wong, K. S.; et al. High-Performance Blue Perovskite Light-Emitting Diodes Enabled by Efficient Energy Transfer between Coupled Quasi-2D Perovskite Layers. *Adv. Mater.* **2021**, *33* (1), e2005570.
(21) Cai, W.; Ali, M. U.; Liu, P.; He, M.; Zhao, C.; Chen, Z.; Zang, Y.; Tang, M.-C.; Meng, H.; Fu, H.; et al. Unravelling Alkali-Metal-Assisted Domain Distribution of Quasi-2D Perovskites for Cascade Energy Transfer toward Efficient Blue Light-Emitting Diodes. *Adv. Sci.* **2022**, *9* (20), 2200393.
(22) Yang, Y.; Xu, S.; Ni, Z.; Van Brackle, C. H.; Zhao, L.; Xiao, X.; Dai, X.; Huang, J. Highly Efficient Pure-Blue Light-Emitting Diodes Based on Rubidium and Chlorine Alloyed Metal Halide Perovskite. *Adv. Mater.* **2021**, *33* (33), e2100783.
(23) Yuan, S.; Cui, L. S.; Dai, L.; Liu, Y.; Liu, Q. W.; Sun, Y. Q.; Auras, F.; Anaya, M.; Zheng, X.; Ruggeri, E.; et al. Efficient and Spectrally Stable Blue Perovskite Light-Emitting Diodes Employing a Cationic pi-Conjugated Polymer. *Adv. Mater.* **2021**, *33* (45), e2103640.
(24) Jang, C. H.; Harit, A. K.; Lee, S.; Kim, S. H.; Jeong, J.-E.; Park, J. H.; Jung, E. D.; Ha, J. M.; Kwak, S. K.; Woo, H. Y.; et al. Sky-Blue-Emissive Perovskite Light-Emitting Diodes: Crystal Growth and Interfacial Control Using Conjugated Polyelectrolytes as a Hole-Transporting Layer. *ACS Nano* **2020**, *14* (10), 13246-13255.
(25) Shen, Y.; Shen, K.-C.; Li, Y.-Q.; Guo, M.; Wang, J.; Ye, Y.; Xie, F.-M.; Ren, H.; Gao, X.; Song, F.; et al. Interfacial Potassium-Guided Grain Growth for Efficient Deep-Blue Perovskite Light-Emitting Diodes. *Adv. Funct. Mater.* **2021**, *31* (6), 2006736.
(26) Chu, Z.; Zhao, Y.; Ma, F.; Zhang, C.-X.; Deng, H.; Gao, F.; Ye, Q.; Meng, J.; Yin, Z.; Zhang, X.; et al. Large cation ethylammonium incorporated perovskite for efficient and spectra stable blue light-emitting diodes. *Nat. Commun.* **2020**, *11* (1), 4165.
(27) Mishra, J. K.; Yantara, N.; Kanwat, A.; Furuhashi, T.; Ramesh, S.; Salim, T.; Jamaludin, N. F.; Febriansyah, B.; Ooi, Z. E.; Mhaisalkar, S.; et al. Defect Passivation Using a Phosphonic Acid Surface

Modifier for Efficient RP Perovskite Blue-Light-Emitting Diodes. *ACS Appl. Mater. & Interfaces* **2022**, *14* (30), 34238-34246.

(28) Ye, S.; Rao, H.; Feng, M.; Xi, L.; Yen, Z.; Seng, D. H. L.; Xu, Q.; Boothroyd, C.; Chen, B.; Guo, Y.; et al. Expanding the low-dimensional interface engineering toolbox for efficient perovskite solar cells. *Nature Energy* **2023**, *8* (3), 284-293.

(29) Li, C.; Wang, X.; Bi, E.; Jiang, F.; Park, S. M.; Li, Y.; Chen, L.; Wang, Z.; Zeng, L.; Chen, H.; et al. Rational design of Lewis base molecules for stable and efficient inverted perovskite solar cells. *Science* **2023**, *379* (6633), 690-694.

(30) Singh, S.; Banappanavar, G.; Kabra, D. Correlation between Charge Transport Length Scales and Dielectric Relaxation Time Constant in Hybrid Halide Perovskite Semiconductors. *ACS Energy Letters* **2020**, *5* (3), 728-735.

(31) Liu, S.; Guo, Z.; Wu, X.; Liu, X.; Huang, Z.; Li, L.; Zhang, J.; Zhou, H.; Sun, L.-D.; Yan, C.-H. Zwitterions Narrow Distribution of Perovskite Quantum Wells for Blue Light-Emitting Diodes with Efficiency Exceeding 15%. *Adv. Mater.* **2023**, *35* (3), 2208078.

(32) Jang, C. H.; Kim, Y. I.; Harit, A. K.; Ha, J. M.; Park, S.; Noh, Y. W.; Lee, A.-y.; Kim, K. S.; Jung, J. W.; Woo, H. Y.; et al. Multifunctional Conjugated Molecular Additives for Highly Efficient Perovskite Light-Emitting Diodes. *Adv. Mater. n/a* (n/a), 2210511.

(33) Shen, X.; Kang, K.; Yu, Z.; Jeong, W. H.; Choi, H.; Park, S. H.; Stranks, S. D.; Snaith, H. J.; Friend, R. H.; Lee, B. R. Passivation strategies for mitigating defect challenges in halide perovskite light-emitting diodes. *Joule* **2023**, *7* (2), 272-308.

(34) Kong, L.; Zhang, X.; Li, Y.; Wang, H.; Jiang, Y.; Wang, S.; You, M.; Zhang, C.; Zhang, T.; Kershaw, S. V.; et al. Smoothing the energy transfer pathway in quasi-2D perovskite films using methanesulfonate leads to highly efficient light-emitting devices. *Nat Commun* **2021**, *12* (1), 1246.

(35) Guo, Z.; Zhang, Y.; Wang, B.; Wang, L.; Zhou, N.; Qiu, Z.; Li, N.; Chen, Y.; Zhu, C.; Xie, H.; et al. Promoting Energy Transfer via Manipulation of Crystallization Kinetics of Quasi-2D Perovskites for Efficient Green Light-Emitting Diodes. *Adv. Mater.* **2021**, *33* (40), 2102246.

(36) Vicentini, G.; Dunstan, P. O. Diphenylphosphinamide adducts of the lanthanide perchlorates. *J. lnorg. Nucl. Chem.* **1971**, *33* (6), 1749-1756.

(37) Ren, Z.; Sun, J.; Yu, J.; Xiao, X.; Wang, Z.; Zhang, R.; Wang, K.; Chen, R.; Chen, Y.; Choy, W. C. H. High-Performance Blue Quasi-2D Perovskite Light-Emitting Diodes via Balanced Carrier Confinement and Transfer. *Nano-Micro Lett.* **2022**, *14* (1), 66.

(38) Li, M.; Zhao, Y.; Qin, X.; Ma, Q.; Lu, J.; Lin, K.; Xu, P.; Li, Y.; Feng, W.; Zhang, W.-H.; et al. Conductive Phosphine Oxide Passivator Enables Efficient Perovskite Light-Emitting Diodes. *Nano Lett.* **2022**, *22* (6), 2490-2496.

(39) Greve, C.; Nibbering, E. T. J.; Fidder, H. Hydrogen-Bonding-Induced Enhancement of Fermi Resonances: A Linear IR and Nonlinear 2D-IR Study of Aniline-d5. *J. Phys. Chem. B* **2013**, *117* (49), 15843-15855.

(40) Liang, X.; Liu, Z.; Zhang, J.; Chen, H.; Gu, Q.; Zhang, W.; Shen, C.; Xiao, Z.; Wang, Y.; Liao, J.; et al. Promoting Energy Transfer Between Quasi-2D Perovskite Layers Toward Highly Efficient Red Light-Emitting Diodes. *Small* **2022**, *18* (49), 2204638.

(41) Ma, D.; Lin, K.; Dong, Y.; Choubisa, H.; Proppe, A. H.; Wu, D.; Wang, Y.-K.; Chen, B.; Li, P.; Fan, J. Z.; et al. Distribution control enables efficient reduced-dimensional perovskite LEDs. *Nature* **2021**, *599* (7886), 594-598.

(42) Zhang, L.; Sun, C.; He, T.; Jiang, Y.; Wei, J.; Huang, Y.; Yuan, M. High-performance quasi-2D perovskite light-emitting diodes: from materials to devices. *Light-sci Appl* **2021**, *10* (1), 61.

(43) Ledinsky, M.; Schönfeldová, T.; Holovský, J.; Aydin, E.; Hájková, Z.; Landová, L.; Neyková, N.; Fejfar, A.; De Wolf, S. Temperature Dependence of the Urbach Energy in Lead Iodide Perovskites. *J. Phys. Chem. Lett.* **2019**, *10* (6), 1368-1373.

(44) Li, L.; Hu, Y.; Chen, Y.; Wang, C.; Zhao, G.; Du, X.; Wang, C.; Xiao, L.; Lu, Z.; Wang, J. Surface Defect Suppression for High Color Purity Light-Emitting Diode of Free-Standing Single-Crystal Perovskite Film. *Adv. Funct. Mater.* **2023**, 2301205.

(45) Luo, Y.; Kong, L.; Wang, L.; Shi, X.; Yuan, H.; Li, W.; Wang, S.; Zhang, Z.; Zhu, W.; Yang, X. A Multifunctional Ionic Liquid Additive Enabling Stable and Efficient Perovskite Light-Emitting Diodes. *Small* **2022**, *18* (19), 2200498.

(46) Xie, M.; Guo, J.; Zhang, X.; Bi, C.; Zhang, L.; Chu, Z.; Zheng, W.; You, J.; Tian, J. High-efficiency pure-red perovskite quantum-dot light-emitting diodes. *Nano Lett.* **2022**, *22* (20), 8266-8273.

(47) Bi, C.; Yao, Z.; Sun, X.; Wei, X.; Wang, J.; Tian, J. Perovskite quantum dots with ultralow trap density by acid etching-driven ligand exchange for high luminance and stable pure-blue light-emitting diodes. *Adv. Mater.* **2021**, *33* (15), 2006722.

(48) Bowman, A. R.; Macpherson, S.; Abfalterer, A.; Frohna, K.; Nagane, S.; Stranks, S. D. Extracting Decay-Rate Ratios From Photoluminescence Quantum Efficiency Measurements in Optoelectronic Semiconductors. *Phys. Rev. Appl.* **2022**, *17* (4), 044026.

(49) Canil, L.; Cramer, T.; Fraboni, B.; Ricciarelli, D.; Meggiolaro, D.; Singh, A.; Liu, M.; Rusu, M.; Wolff, C. M.; Phung, N.; et al. Tuning halide perovskite energy levels. *Energy Environ. Sci.* **2021**, *14* (3), 1429-1438, 10.1039/D0EE02216K.

(50) Kim, H.; Kim, J. S.; Heo, J.-M.; Pei, M.; Park, I.-H.; Liu, Z.; Yun, H. J.; Park, M.-H.; Jeong, S.-H.; Kim, Y.-H.; et al. Proton-transfer-induced 3D/2D hybrid perovskites suppress ion migration and reduce luminance overshoot. *Nat. Commun.* **2020**, *11* (1), 3378.

(51) Zhang, D.; Fu, Y.; Zhan, H.; Zhao, C.; Gao, X.; Qin, C.; Wang, L. Suppressing thermal quenching via defect passivation for efficient quasi-2D perovskite light-emitting diodes. *Light Sci Appl* **2022**, *11* (1), 69.